4-12-2010

Commensuration and Interlayer Coherence in Twisted Bilayer Graphene

Eugene J. Mele
University of Pennsylvania, mele@physics.upenn.edu

Suggested Citation:
Mele, E.J. (2010). "Commensuration and interlayer coherence in twisted bilayer graphene." *Physical Review B.* 81, 161405(R).

http://dx.doi.org/10.1103/PhysRevB.81.161405

Commensuration and Interlayer Coherence in Twisted Bilayer Graphene

Abstract

The low-energy electronic spectra of rotationally faulted graphene bilayers are studied using a longwavelength theory applicable to general commensurate fault angles. Lattice commensuration requires lowenergy electronic coherence across a fault and pre-empts massless Dirac behavior near the neutrality point. Sublattice exchange symmetry distinguishes two families of commensurate faults that have distinct low-energy spectra which can be interpreted as energy-renormalized forms of the spectra for the limiting Bernal and *AA* stacked structures. Sublattice-symmetric faults are generically fully gapped systems due to a pseudospin-orbit coupling appearing in their effective low-energy Hamiltonians.

Disciplines

Physical Sciences and Mathematics | Physics

Comments

Suggested Citation:
Mele, E.J. (2010). "Commensuration and interlayer coherence in twisted bilayer graphene." *Physical Review B.* 81, 161405(R).

http://dx.doi.org/10.1103/PhysRevB.81.161405

PHYSICAL REVIEW B **81**, 161405(R) (2010)

Commensuration and interlayer coherence in twisted bilayer graphene

E. J. Mele*
Department of Physics and Astronomy, University of Pennsylvania, Philadelphia, Pennsylvania 19104, USA
(Received 22 March 2010; published 12 April 2010)

The low-energy electronic spectra of rotationally faulted graphene bilayers are studied using a long-wavelength theory applicable to general commensurate fault angles. Lattice commensuration requires low-energy electronic coherence across a fault and pre-empts massless Dirac behavior near the neutrality point. Sublattice exchange symmetry distinguishes two families of commensurate faults that have distinct low-energy spectra which can be interpreted as energy-renormalized forms of the spectra for the limiting Bernal and *AA* stacked structures. Sublattice-symmetric faults are generically fully gapped systems due to a pseudospin-orbit coupling appearing in their effective low-energy Hamiltonians.

DOI: 10.1103/PhysRevB.81.161405 PACS number(s): 73.20.−r

Coherent interlayer electronic motion in multilayer graphenes play a crucial role in their low-energy properties.[1] This physics is well understood for stacked structures with neighboring crystallographic axes rotated by multiples of $\pi/3$, including *AB* (Bernal), *AA*, *ABC* stackings, and their related polymorphs.[2] Here the interlayer coupling scale typically exceeds 0.5 eV and pre-empts the massless Dirac physics of an isolated graphene sheet. Indeed experimental work on Bernal stacked bilayers[3–6] demonstrates that their electronic properties are radically different from those of a single layer.[7,8] Yet, recent experimental work has revealed a family of multilayer graphenes that show only weak (if any) effects of their interlayer interaction. These include graphenes grown epitaxially on the SiC$(000\bar{1})$ surface,[9–11] mechanically exfoliated folded graphene bilayers,[12] and graphene flakes deposited on graphite.[13] A common structural attribute of these systems is the rotational misorientation of their neighboring layers at angles $\theta \neq n\pi/3$. A continuum theoretic model has suggested that misorientation by an arbitrary fault angle induces a momentum mismatch between the tips of the Dirac cones in neighboring layers suppressing coherent interlayer motion at low energy.[14] In this interpretation, the Dirac points of neighboring layers remain quantum mechanically *decoupled* across a rotational fault[11,14–18] accessing two-dimensional physics in a family of three-dimensional materials.

This Rapid Communication presents a long-wavelength theory of electronic motion in graphene bilayers containing rotational faults at arbitrary commensurate angles. I find that the Dirac nodes of these structures are directly coupled across any commensurate rotational fault, producing unexpectedly rich physics near their charge neutrality points. The theory generalizes previous approximate analyses[14] by treating the lateral modulation of the interlayer coupling between rotated layers which is essential for understanding the low-energy physics. Importantly, commensurate rotational faults occur in two distinct forms distinguished by their sublattice parity. Structures that are even under sublattice exchange (SE) are generically gapped (nonconducting) materials while those that break SE symmetry have two massive (curved) bands contacted at discrete Fermi points. Both these behaviors derive from the spectral properties of *AA* and Bernal stacked structures, and can be understood as energy-renormalized versions of these limiting cases. The gap in the faulted sublattice-symmetric states appears as a new feature specific to the faulted structures due to a pseudospin dependence of the transmission amplitude across a twisted bilayer. These results provide the appropriate low-energy Hamiltonian(s) for rotationally faulted bilayers superseding the massless Dirac model of an isolated sheet.

The crystal structure of two-dimensional graphene (Fig. 1) has a Bravais lattice spanned by two primitive translations $t_1 = e^{-i\pi/6}$ and $t_2 = e^{i\pi/6}$ with sublattice sites at $\tau_{A(B)} = 0(1/\sqrt{3})$. We consider rotational stacking faults that fix overlapping *A*-sublattice sites at the origin and rotate one layer through angle θ with respect to the other with translation vectors $(t_1', t_2') = e^{i\theta}(t_1, t_2)$ and basis $\tau_{A(B)}' = e^{i\theta}\tau_{A(B)}$. A commensurate rotation occurs when $T_{m,n} = mt_1 + nt_2 = m't_1' + n't_2' = T_{m',n'}'$ which is generically satisfied by angles indexed by two integers m and n with $\theta(m,n) = \arg[(me^{-i\pi/6} + ne^{i\pi/6})/(ne^{-i\pi/6} + me^{i\pi/6})]$. In this notation *AA* stacking (all sites in neighboring layers eclipsed) has $\theta = 0$ and Bernal stacking has $\theta = \pi/3$. Small angular deviations from the Bernal structure have indices $m = 1$ and large n. The $\sqrt{13} \times \sqrt{13}$ structures with $\theta = 30° \pm 2.204°$ structures observed by electron diffraction from epitaxial graphene on the Si$(000\bar{1})$ face correspond to $(m,n) = (1,3)$ and $(m,n) = (2,5)$.[19]

Commensurate faults occur in two families determined by their SE symmetry. With the *A*-sublattice sites at the origin, a commensuration is SE symmetric if *B*-sublattice sites are coincident at some other lattice position in the primitive cell.

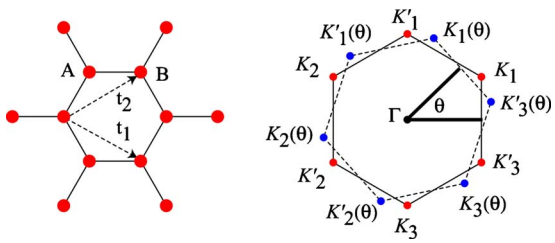

FIG. 1. (Color online) (Left) Lattice structure of graphene with two sites in the primitive cell (*A* and *B*) and primitive translations t_1 and t_2. (Right) Brillouin zones for the two layers in a rotational fault: the Brillouin-zone corners labeled K_m and K_m' are rotated by angle θ to the points $K_m(\theta)$ and $K_m'(\theta)$ in the neighboring layer.

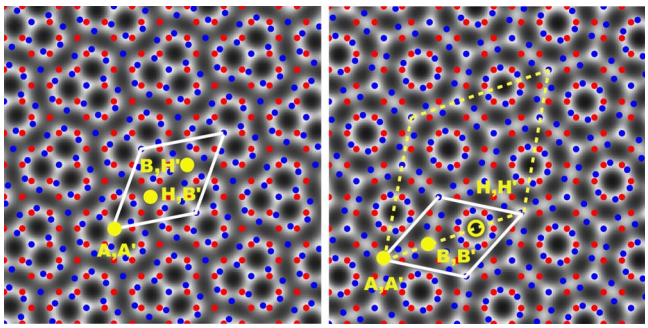

FIG. 2. (Color online) Geometry of the commensuration cells for bilayers faulted at 21.787° (left) and 38.213° (right). Red and blue dots denote the atom positions in the two layers. The white rhombuses denote primitive commensuration cells with the same area for these two structures. The dashed yellow rhombus denotes a $\sqrt{3}\times\sqrt{3}$ nonprimitive cell. The left-hand structure is SE odd, with coincident atomic sites only on the $A(A')$ sublattice at the origin, the right-hand structure is SE even with coincident sites on the $A(A')$ and $B(B')$ sublattices at threefold-symmetric positions in the primitive cell and overlapping hexagon centers (H,H'). The density plot gives the magnitude of the interlayer hopping potential discussed in the text.

This occurs when $\tau_B+T_{p,q}=\tau_{B'}+T'_{p',q'}$ for integers (p,q) and (p',q'), requiring integer solutions to $p=(m-n+3mq)/(3n)$. This occurs only when $m-n$ is divisible by 3 and then the coincident $B(B')$ sublattice site occurs at one of the three possible threefold-symmetric positions of the cell (e.g., $T_{m,n}/3$ in Fig. 2). The remaining threefold positions are occupied by the $A(A')$-sublattice sites (the origin) and by overlapping hexagon centers (H,H'). When $m-n$ is not divisible by 3 the only coincident site is the A site at the origin and the remaining two threefold-symmetric positions are occupied by B-sublattice atoms of one layer aligned with the hexagon centers (H') of its neighbor. Rotational faults at angles $\bar{\theta}=\pi/3-\theta$ form commensuration partners with primitive cells of equal areas but opposite sublattice parities. Figure 2 illustrates this situation for two partner commensurations at $30°-8.213°$ $[(m,n)=(1,2)]$ (left) and $30°+8.213°$ $[(m,n)=(1,4)]$ (right). The limiting cases of Bernal (odd) and AA (even) stackings form the shortest period commensuration pair.

Because of the rotation, the Brillouin zones of the two layers have different orientations [Fig. 1(b)] shifting their zone corners (K_m,K'_m) to rotated counterparts $[K_m(\theta),K'_m(\theta)]$. The low-energy electronic bands of the decoupled layers have isotropic conical dispersions near each of these points with $E(q)=\pm\hbar v_F|q|$, where q is the crystal momentum measured relative to the corner and v_F is the Fermi velocity. These spectra are described by a pair of massless Dirac Hamiltonians for the K and K' points of the two layers.[21] Interlayer coupling is studied using a long-wavelength theory that represents the low-energy states as spatially modulated versions of the orthogonal zone corner Bloch states of the two layers, i.e., $\Psi(\vec{r})=\Sigma_\alpha\psi_{K,\alpha}(\vec{r})u_\alpha(\vec{r})$. By retaining the reciprocal-lattice vectors that constrain the sum in $\psi_{K,\alpha}$ to the three equivalent corners of the Brillouin zone we obtain the Bloch states $\psi_{K,\alpha}=(1/\sqrt{3})\Sigma_m e^{i\vec{K}_m\cdot(\vec{r}-\vec{\tau}_\alpha)}$. The coupling between layers is derived from an interaction functional which correlates the amplitudes and phases of the Bloch states in neighboring layers

$$U=(1/2)\int d^2rT_\ell(\vec{r})|\Psi_1(\vec{r})-\Psi_2(\vec{r})|^2, \tag{1}$$

where T_ℓ is a supercell-periodic modulation of the coupling due to the lattice structure of the commensuration cell. Using Eq. (1) one finds that the interlayer coupling is expressed in terms of the Fourier transforms of the smooth fields u_α,

$$\frac{U_{\rm int}}{N}=\frac{\mathcal{A}_o}{24\pi^2}\int d^2q\sum_{\alpha,\beta}\sum_{m;m'}e^{i\vec{K}_m\cdot\vec{\tau}_\alpha}e^{-i\vec{K}_{m'}\cdot\vec{\tau}'_\beta}\times\sum_{\vec{\mathcal{G}}}[t(\vec{\mathcal{G}})u^*_{1,\alpha}(\vec{q})u_{2,\beta}(\vec{q}+\vec{K}_m-\vec{K}_{m'}-\vec{\mathcal{G}})+\text{c.c.}], \tag{2}$$

where N is the system size, $\mathcal{A}_o$ is the area of a graphene primitive cell, and $t(\vec{\mathcal{G}})$ is the Fourier transform of the interlayer potential $T_\ell(\vec{r})$ on the reciprocal lattice of the commensuration cell $\vec{\mathcal{G}}$.

The continuum theory of Ref. 14 is recovered from Eq. (2) by retaining only its $\vec{\mathcal{G}}=0$ terms, thus treating the interlayer coupling as *spatially uniform*. In this approximation the states near the tip of the Dirac cone in one layer are coupled to three pairs of states at energies $\pm W^*=\pm\hbar v_F|K_m-K_m(\theta)|$ in its neighbor. At low energies this coupling can be treated perturbatively, preserving the Dirac nodes of two isotropic velocity-renormalized layer-decoupled Hamiltonians.

Different physics arises from the $\vec{\mathcal{G}}\neq 0$ contributions to Eq. (2) which mediate a direct coupling between the Dirac nodes of neighboring layers and prevent massless low-energy behavior. To study it, note that the reciprocal lattice of the bilayer is spanned by momenta with *four* integer indices $\vec{\mathcal{G}}=p\vec{G}_1+q\vec{G}_2+p'\vec{G}'_1+q'\vec{G}'_2$.[20] Momentum conserving couplings between K points in neighboring layers occur when $K_m-K_{m'}(\theta)=\vec{\mathcal{G}}(p,q,p',q')$ with the angle $\theta(m,n)$ specified. This is an *interlayer umklapp* process where the spatial modulation of $T_\ell(\vec{r})$ provides precisely the transverse momentum required to transport an electron between the Dirac nodes of neighboring layers. The momentum matching condition requires integer p solutions to $p=(m-n)/3n+qm/n$ and occurs only for *supercommensurate* structures with nonzero $\text{mod}(m,3)=\text{mod}(n,3)$. Importantly if this condition is not satisfied, momentum-conserving interlayer couplings still occur, but instead through the analogous *intervalley* umklapp process, i.e., $K'_m-K_{m'}(\theta)=\vec{\mathcal{G}}(p,q,p',q')$. These two possibilities are complementary and mutually exclusive: one or the other must occur if the rotational fault is commensurate. These two criteria distinguish SE-even and SE-odd structures so that the SE-even structures require direct $K-K(\theta)$ coupling and SE-odd structures $K-K'(\theta)$ coupling.

To understand the consequences of the interlayer interaction one requires a theory for the Fourier coefficients $t(\vec{\mathcal{G}})$ in Eq. (2). These can be calculated from atomistic models but their relevant properties are determined by symmetry. Note that the coupling function $T_\ell(\vec{r})$ is a real periodic function

with the translational symmetry of the commensuration cell. The structure function for the μth layer, $n_\mu(\vec{r}) = \sum_{m\in[1]}\sum_\alpha e^{i\vec{G}_{\mu,m}\cdot(\vec{r}-\vec{\tau}_{\mu,\alpha})}$ superposes the six plane waves of the lowest star of reciprocal-lattice vectors $\vec{G}_{\mu,m}$ producing a standing wave with maxima on atom sites and minima in hexagon centers. A useful model for the interlayer coupling potential is $T_\ell(\vec{r}) = C_0 \exp[C_1 n(\vec{r})]$, where $n(\vec{r}) = n_1 + n_2$ and C_0 and C_1 are constants; T_ℓ is a superlattice-periodic function with maxima for coincident sites and with exponential suppression in regions that are out of interlayer registry. The grayscale plot in Fig. 2 show the spatial distribution of $T_\ell(\vec{r})$, where C_1 is determined by matching the decay of the hopping amplitude between neighboring layer atoms as a function of small lateral offsets. This density plot shows that the interlayer amplitudes between rotated layers have coherent structures in the forms of fivefold rings (from overlapping misaligned hexagons) arranged to form two-dimensional space-filling patterns. SE-odd structures are symmetric under threefold rotations while the SE-even structures retain a sixfold symmetry. The separable form $T_\ell(\vec{r}) = f_1(\vec{r}) f_2(\vec{r})$ allows one to deduce a scaling rule for the Fourier coefficients: $t(\vec{\mathcal{G}}) \approx (a e^{-b/N_c}/N_c)\Sigma_{\mu\in[1]} f_2(\vec{r}_\mu) e^{-i\vec{\mathcal{G}}\cdot\vec{r}_\mu}$, where the sum is over atomic sites in layer 1, a and b are constants, and N_c is the number of graphene cells (per layer) in the commensuration cell. For large N_c the prefactor decays as a power law of the cell size reflecting the fraction of atomic sites in good interlayer registry while the sum decays quickly as a function of N_c because of canceling phases in its argument.

The interlayer Hamiltonian can be expressed by a 3×3 array of scattering amplitudes derived from the $t(\vec{\mathcal{G}})$'s giving the allowed transitions $K_m \to K_{m'}(\theta)$. Threefold symmetry requires this matrix to have the form

$$\hat{\mathcal{V}}_{\rm ps} = \begin{pmatrix} V_0 & V_1 & V_2 \\ V_2 & V_0 & V_1 \\ V_1 & V_2 & V_0 \end{pmatrix},$$

where the pseudopotential coefficients V_i are matrix elements of T_ℓ. Completing the sum in Eq. (2) transforms this to the sublattice (pseudospin) basis and gives the 2×2 interlayer transition matrices $\hat{\mathcal{H}}_{\rm int}$ seen by the Dirac fermions. The low-energy Hamiltonian for an SE-even bilayer is expressed as a 4×4 matrix (acting on the two sublattice and two layer degrees of freedom),

$$\hat{\mathcal{H}}_{\rm even} = \begin{pmatrix} -i\hbar\tilde{v}_F \boldsymbol{\sigma}_1\cdot\nabla & \hat{\mathcal{H}}^+_{\rm int} \\ (\hat{\mathcal{H}}^+_{\rm int})^\dagger & -i\hbar\tilde{v}_F \boldsymbol{\sigma}_2\cdot\nabla \end{pmatrix} \tag{3}$$

and for the SE-odd bilayer

$$\hat{\mathcal{H}}_{\rm odd} = \begin{pmatrix} -i\hbar\tilde{v}_F \boldsymbol{\sigma}_1\cdot\nabla & \hat{\mathcal{H}}^-_{\rm int} \\ (\hat{\mathcal{H}}^-_{\rm int})^\dagger & i\hbar\tilde{v}_F \boldsymbol{\sigma}_2^*\cdot\nabla \end{pmatrix}, \tag{4}$$

where σ_n are Pauli matrices acting in the sublattice pseudospin basis of the nth layer and $\tilde{v}_F$ is the renormalized Fermi velocity. The interlayer matrices $\hat{\mathcal{H}}^\pm_{\rm int}$ are

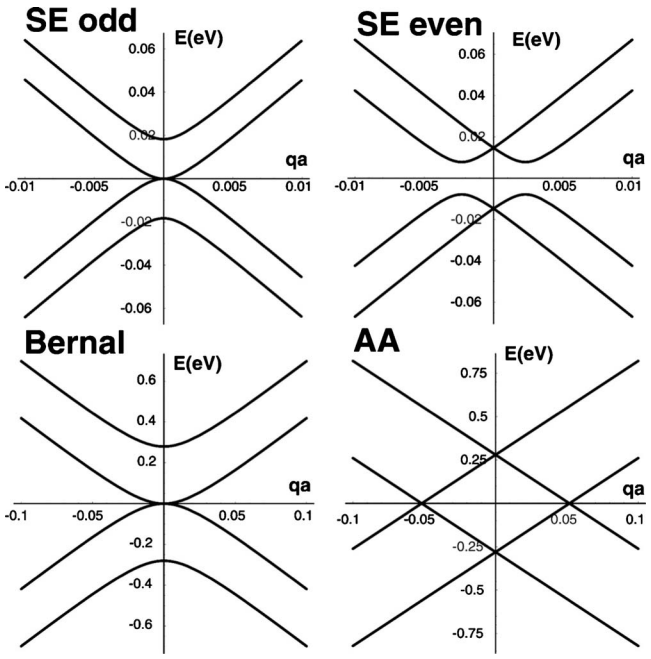

FIG. 3. Low-energy electronic spectra for SE-odd and SE-even faulted bilayers are illustrated using partner commensurations at rotation angles $\theta = 21.787°$ (odd, left) and $\theta = 38.213°$ (even, right). These spectra are symmetric under rotations in momentum space. SE-odd faults have massive bands that contact at Fermi points (left) and SE-even faults are gapped (right). The lower row gives the spectrum for a Bernal bilayer (left) and for an *AA* bilayer, which show related spectral properties.

$$\hat{\mathcal{H}}^+_{\rm int} = \mathcal{V} e^{i\vartheta}\begin{pmatrix} e^{i\varphi/2} & 0 \\ 0 & e^{-i\varphi/2} \end{pmatrix}, \quad \hat{\mathcal{H}}^-_{\rm int} = \mathcal{V} e^{i\vartheta}\begin{pmatrix} 1 & 0 \\ 0 & 0 \end{pmatrix}. \tag{5}$$

$\hat{\mathcal{H}}^+_{\rm int}$ shows that interlayer motion of an electron for SE-even faults involves an intravalley transition with a unitary transformation of its (A,B) sublattice amplitudes represented as an *xy rotation of its pseudospin through angle* φ. This angle is *not* defined geometrically by the fault angle θ but rather is determined by the relative magnitudes of the three pseudopotential matrix elements V_i. By contrast interlayer motion across a sublattice asymmetric fault requires an intervalley transition through only the amplitudes on its dominant (eclipsed) sublattice. The continuum model of Ref. 14 is recovered by setting $\hat{\mathcal{H}}_{\rm int} = 0$.

In either case, below an energy scale $\mathcal{V}$ the electronic spectra deviate from the massless Dirac form and inherit curvature from the interlayer coupling as shown in Fig. 3. $\mathcal{V} \sim 10$ meV for commensurations at $\theta = 30° \pm 8.213°$ with $N_c = 7$ graphene cells per layer in their commensuration cells. Nevertheless the forms of these spectra apply generally to any pair of commensuration partners. SE-odd faults mix the degenerate Dirac bands gapping one pair on the scale $\mathcal{V}$, leaving a second pair of massive (curved) bands in contact at $E = 0$. By contrast, SE even structures are fully gapped where the gap arises entirely from the pseudospin rotation in Eq. (5). Indeed for $\varphi = 0$ these spectra consist of a pair of Dirac cones offset in energy by a bonding-antibonding splitting and

intersecting at $E=0$ on a circle in reciprocal space. The pseudospin rotation lowers the symmetry of the bilayer and produces an avoided crossing of these states. For SE-even rotated bilayers the interlayer coupling describes a type of spin-orbit coupling with the sublattice pseudospin index playing the role of the spin.

These behaviors have precise analogs for the limiting cases of unfaulted Bernal and *AA* stacked layers. The Bernal bilayer (lower left Fig. 3) has exactly the structure found for SE-odd faults but on an inflated energy scale ~ 0.5 eV, reflecting the full alignment of all atoms on a single sublattice. Similarly, for *AA* bilayers (lower right Fig. 3) interacting Dirac cones are displaced in energy but *without* a pseudospin rotation, so they intersect on rings at $E=0$. All intermediate commensurate site-centered rotational faults display either energy-renormalized Bernal-type or *AA*-like low-energy spectra; the reduction in the energy scale is a measure of the loss of interlayer registry in the faulted bilayer. This correspondence can be deduced from the lattice symmetries of the density plots shown in Fig. 2.

Since $\mathcal{V}<W^*$ rotational faults open an energy "window" $\mathcal{V}<E<W^*$ in which the physics is well described by decoupled two-dimensional systems before their interlayer coherence is apparent. The theory of small angular deviations from Bernal stacking[14] can be understood as a collapse of the energy scale $\mathcal{V}$ relative to W^*. Yet, physics at the scale $\mathcal{V}$ is accessible to experimental probes and highly relevant to electrostatic gating and charge transport in structures derived from multilayer graphenes[5,12] particularly those with faults near $\theta=\pi/6$ found in epitaxial graphenes on SiC$(000\bar{1})$.[11] Additionally, the many-body physics of these systems depends crucially on the low-energy structure of these spectra[22] and it can be expected to be quite different for different stacking sequences. Thus one can regard faulted multilayer graphenes as presenting a family of new materials with properties that interpolate between single-layer graphene and bulk graphite in an understandable and hopefully controllable way.

I thank C. L. Kane, S. Kim, and A. M. Rappe for their helpful comments. This work was supported by the Department of Energy under Grant No. DE-FG02-ER45118.

*mele@physics.upenn.edu

[1] J. W. McClure, Phys. Rev. **108**, 612 (1957).
[2] H. Min and A. H. MacDonald, Phys. Rev. B **77**, 155416 (2008).
[3] E. McCann and V. I. Fal'ko, Phys. Rev. Lett. **96**, 086805 (2006).
[4] T. Ohta, A. Bostwick, T. Seyller, K. Horn, and E. Rotenberg, Science **313**, 951 (2006).
[5] E. V. Castro, K. S. Novoselov, S. V. Morozov, N. M. R. Peres, J. M. B. Lopes dos Santos, J. Nilsson, F. Guinea, A. K. Geim, and A. H. Castro Neto, Phys. Rev. Lett. **99**, 216802 (2007).
[6] Z. Q. Li, E. A. Henriksen, Z. Jiang, Z. Hao, M. C. Martin, P. Kim, H. L. Stormer, and D. N. Basov, Phys. Rev. Lett. **102**, 037403 (2009).
[7] K. S. Novoselov, A. K. Geim, S. V. Morozov, D. Jiang, M. I. Katsnelson, I. V. Grigorieva, S. V. Dubonos, and A. A. Firsov, Nature (London) **438**, 197 (2005).
[8] Y. Zhang, Y.-W. Tan, H. L. Stormer, and P. Kim, Nature (London) **438**, 201 (2005).
[9] C. Berger, Z. Song, X. Li, X. Wu, N. Brown, C. Naud, D. Mayou, T. Li, J. Hass, A. N. Marchenkov, E. H. Conrad, P. N. First, and W. A. de Heer, Science **312**, 1191 (2006).
[10] J. Hass, R. Feng, J. E. Millán-Otoya, X. Li, M. Sprinkle, P. N. First, W. A. de Heer, E. H. Conrad, and C. Berger, Phys. Rev. B **75**, 214109 (2007).
[11] J. Hass, F. Varchon, J. E. Millán-Otoya, M. Sprinkle, N. Sharma, W. A. de Heer, C. Berger, P. N. First, L. Magaud, and E. H. Conrad, Phys. Rev. Lett. **100**, 125504 (2008).
[12] H. Schmidt, T. Ludtke, P. Barthold, E. McCann, V. I. Fal'ko, and R. J. Haug, Appl. Phys. Lett. **93**, 172108 (2008).
[13] G. Li, A. Luican, and E. Y. Andrei, Phys. Rev. Lett. **102**, 176804 (2009).
[14] J. M. B. Lopes dos Santos, N. M. R. Peres, and A. H. Castro Neto, Phys. Rev. Lett. **99**, 256802 (2007).
[15] S. Latil, V. Meunier, and L. Henrard, Phys. Rev. B **76**, 201402(R) (2007).
[16] J. M. Campanera, G. Savini, I. Suarez-Martinez, and M. I. Heggie, Phys. Rev. B **75**, 235449 (2007).
[17] S. Shallcross, S. Sharma, and O. A. Pankratov, Phys. Rev. Lett. **101**, 056803 (2008).
[18] G. Trambly de Laissardière, D. Mayou, and L. Magaud, Nano Lett. **10**, 804 (2010).
[19] This is indexed to a nonprimitive two-dimensional cell. The related *structural* primitive cell is obtained by using the deflation rule: $(m_p,n_p)=(m-n,m+2n)/3$ giving $(m_p,n_p)=(-1,4)$ which has the same area as the $(m,n)=(1,3)$ cell.
[20] $\vec{G}_i$ and $\vec{G}'_j$ are primitive reciprocal-lattice vectors of each sheet. One could also index $\vec{\mathcal{G}}$ using two primitive reciprocal-lattice vectors dual to the full commensuration cell but the four-index formulation is more powerful.
[21] D. P. DiVincenzo and E. J. Mele, Phys. Rev. B **29**, 1685 (1984).
[22] H. Min, R. Bistritzer, J.-J. Su, and A. H. MacDonald, Phys. Rev. B **78**, 121401(R) (2008).